

A Continuous Galactic Line Source of Axions: The Remarkable Case of ^{23}Na

W. C. Haxton,^{1,2,3, a} Xing Liu,^{1, b} Annie McCutcheon,^{4, c} and Anupam Ray^{1, d}

¹*Department of Physics, University of California, Berkeley, CA 94720, USA*

²*Institute for Nuclear Theory, University of Washington, Seattle, WA 98195, USA*

³*Lawrence Berkeley National Laboratory, Berkeley, CA 94720, USA*

⁴*Department of Physics, University of California, Davis, CA 95616, USA*

(Dated: November 27, 2025)

We argue that ^{23}Na is a potentially significant source of galactic axions. For temperatures $\gtrsim 7 \times 10^8 \text{K}$ – characteristic of carbon burning in the massive progenitors of supernovae and ONeMg white dwarfs – the 440 keV first excited state of ^{23}Na is thermally populated, with its repeated decays pumping stellar energy into escaping axions. Odd- A nuclear abundances are typically very low in high-temperature stellar environments (or absent entirely due to burn-up). ^{23}Na is an exception: $\approx 0.1M_\odot$ of the isotope is synthesized during carbon burning then maintained at $\approx 10^9 \text{K}$ for times ranging up to $6 \times 10^4 \text{y}$. Using MESA simulations, a galactic model, and sampling over progenitor masses, locations, and evolutionary stages, we find a continuous flux at Earth of $\langle \phi_a \rangle \approx 22/\text{cm}^2 \text{s}$ for $g_{aNN}^{\text{eff}} = 10^{-9}$. Some fraction of these axions converts to photons as they propagate through the galactic magnetic field, producing a distinctive 440 keV line γ -ray detectable by all-sky detectors like the Compton Spectrometer and Imager (COSI). Assuming a $1\mu\text{G}$ galactic magnetic field and a sufficiently light axion mass, we find that COSI will be able to probe $|g_{aNN}^{\text{eff}} g_{a\gamma\gamma}| \gtrsim 1.8 \times 10^{-22} \text{GeV}^{-1}$ at 3σ after two years of surveying.

In 1977 Peccei and Quinn proposed a solution [1] to the strong CP problem that depended on the introduction of a new scalar field. Soon after, Weinberg [2] and Wilczek [3] independently observed that a consequence of the Peccei–Quinn mechanism would be a new particle, the axion. Currently the axion is one of the most popular candidates for the dark matter, albeit characterized by couplings to standard-model particles considerably weaker than those originally envisioned.

Many of the existing constraints on axion-matter couplings depend on astrophysical sources. A celebrated example is the early universe, where axions are produced from the harmonic oscillations of the axion potential as it seeks its minimum, damping that motion. Sikivie [4, 5] proposed that cosmological axions could be observed through their conversion to microwave photons of the same energy. ADMX is searching for these conversion photons, using a magnetic cavity tuned to absorb the missing momentum [6–9]. Various related experiments are underway [10–14]. Axions or axion-like particles (ALPs) are a potential source of X-rays from both young [15–20] and older [21–23] neutron stars. ALPs can alter the cooling of various stars [24, 25], including transient events like supernovae [26–30].

An interesting astrophysical source was pointed out by Haxton and Lee [31]: certain nuclei with low-lying M1 transitions can serve as axion pumps, converting stellar thermal energy into axions through repeated photo-excitation and axio-deexcitation. They studied this mechanism as a function of stellar core temperature (T), identifying three isotopes of special importance. At low temperatures $T_8 = T/10^8 \text{K} \approx 1$, ^{57}Fe (2.2% of natural Fe) dominates due to its 14.4 keV excited state, made famous by Mossbauer spectroscopy. As this temperature is characteristic of red giants, they used such stars to probe

the hadronic axion “Turner window” [32].

Although the Sun is a poor source of ^{57}Fe axions due to its cool core $T_8 \approx 0.15$, the suppressed Boltzmann occupation of the excited state is mitigated by the Sun’s proximity. The thermally broadened line of ^{57}Fe axions can then be detected on Earth [33] by the inverse resonant process $a + ^{57}\text{Fe} \rightarrow ^{57}\text{Fe}^* \rightarrow ^{57}\text{Fe} + \gamma$. Searches have been conducted by the CAST Collaboration [34] as well as other groups [35–39]. The “axion helioscope” detector exploits $a \rightarrow \gamma$ conversion as axions pass through a strong magnetic field. White dwarfs possessing high core temperatures and strong magnetic fields have also been used as sources and converters of ^{57}Fe axions [40].

Haxton and Lee identified another isotope, ^{23}Na , as the dominant axion pump for high temperatures $T_8 \approx 10$, though this observation has drawn little attention. Here we show that ^{23}Na is the strongest continuous source of line axions in the galaxy. As these axions traverse the galactic magnetic field, they produce a distinctive gamma ray signal, ideal for telescopes like COSI [41].

The ALP-nucleon interaction is

$$\begin{aligned} \mathcal{L} &= \frac{1}{2m_N} \bar{N} \gamma^\mu \gamma_5 (g_{aNN}^0 + g_{aNN}^3 \tau_3) N \partial_\mu a \quad (1) \\ &= \frac{1}{2m_N} \bar{N} \gamma^\mu \gamma_5 \left[g_{app} \left(\frac{1+\tau_3}{2} \right) + g_{ann} \left(\frac{1-\tau_3}{2} \right) \right] N \partial_\mu a \end{aligned}$$

where τ_3 is the third component of isospin, with $g_{app} = g_{aNN}^0 + g_{aNN}^3$ and $g_{ann} = g_{aNN}^0 - g_{aNN}^3$. For the KSVZ [42, 43] and DFSZ [44, 45] QCD axions, the couplings are related to the axion mass scale f_a [46],

$$\left. \begin{array}{l} g_{app}^{\text{KSVZ}} \\ g_{ann}^{\text{KSVZ}} \end{array} \right\} = \frac{m_N}{f_a} \left\{ \begin{array}{l} -0.47 \\ -0.02 \end{array} \right.$$

$$\left. \begin{array}{l} g_{app}^{\text{DFSZ}} \\ g_{ann}^{\text{DFSZ}} \end{array} \right\} = \frac{m_N}{f_a} \left\{ \begin{array}{l} -0.182 - 0.435 \sin^2 \beta \\ -0.160 + 0.414 \sin^2 \beta \end{array} \right. \quad (2)$$

where the angle β is defined as in [24]. The constraint derived from axion cooling of SN1987A [24]

$$[(g_{app} + 0.435g_{ann})^2 + 1.45g_{ann}^2]^{1/2} < 1.19 \times 10^{-9} \quad (3)$$

sets the scale of 10^{-9} used in this study.

Source	ΔE (keV)	T range	B(M1)	g_{aNN}^{eff}
^{57}Fe	14.4	$\lesssim 1.5T_8$	0.0082	$g_{ann} + 0.088 g_{app}$
^{23}Na	440.2	$\gtrsim 4.1T_8$	0.225	$g_{app} - 0.062 g_{ann}$

TABLE I. Comparative properties of the axion emitters ^{57}Fe and ^{23}Na . The temperature range defines where these metals could dominate axion emission from stars.

Equation (2) generates a nuclear amplitude proportional to the Pauli spin operator, so that the allowed nuclear transitions are M1. To minimize nuclear structure uncertainties, the axion decay rate is expressed in terms of the known gamma decay rate [31],

$$\frac{\omega_a}{\omega_\gamma} = \frac{1}{2\pi\alpha} \frac{1}{1 + \delta^2} \left[\frac{g_{aNN}^0 \beta + g_{aNN}^3}{(\mu_0 - \frac{1}{2})\beta + \mu_1 - \eta} \right]^2 \quad (4)$$

where δ is the E2/M1 mixing ratio, and $\mu_0 = 0.88$ and $\mu_1 = 4.706$ are the isoscalar and isovector nucleon magnetic moments, respectively. The nuclear physics input is limited to two ratios of reduced matrix elements

$$\beta \equiv \frac{\langle J_f \| \sum_{i=1}^A \boldsymbol{\sigma}(i) \| J_i \rangle}{\langle J_f \| \sum_{i=1}^A \boldsymbol{\sigma}(i) \tau_3(i) \| J_i \rangle}, \quad \eta \equiv - \frac{\langle J_f \| \sum_{i=1}^A \boldsymbol{\ell}(i) \tau_3(i) \| J_i \rangle}{\langle J_f \| \sum_{i=1}^A \boldsymbol{\sigma}(i) \tau_3(i) \| J_i \rangle} \quad (5)$$

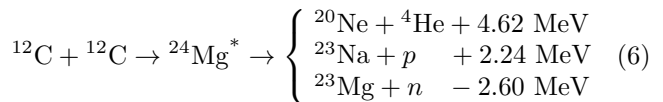
which were evaluated in [31] for cases of interest.

This mechanism requires a low-lying excited state that can be thermally populated under stellar conditions. For example, the Boltzmann occupation of the ^{57}Fe 14.4 keV state at red giant temperatures ($T_8 \approx 1$) is 0.27. The corresponding occupation at solar temperatures, obtained by averaging over the solar core, is just 5×10^{-6} .

Among the three axion emitters discussed in [31], ^{23}Na has the most favorable nuclear physics. Table I compares ^{23}Na and ^{57}Fe . The ^{23}Na B(M1) value – the magnetic transition probability – is a significant fraction of a single-particle unit, nearly 30 times stronger than in ^{57}Fe . In addition, ^{23}Na has an unpaired proton, while ^{57}Fe has a valence neutron. Proton couplings are favored: the KSVZ axion gives $(g_{app}/g_{ann})^2 \approx 550$, while the ratio can range up to infinity for the DFSZ axion, depending on β . The shell-model prediction for the effective nucleon coupling in ^{23}Na is $g_{aNN}^{\text{eff}} = g_{app} - 0.062 g_{ann}$.

^{23}Na also has significant astrophysical advantages. First is its abundance. The Sun's ^{57}Fe is primordial, incorporated at the time of formation: the core contains $7.7 \times 10^{-6} M_\odot$ of ^{57}Fe . By contrast, ^{23}Na is produced *in situ* in carbon-burning massive stars, at temperatures $7 \lesssim T_8 \lesssim 13$. The total mass synthesized is typically $\approx 0.1 M_\odot$. As these temperatures are maintained for times that range up to 60,000 y, several hundred galactic sources may be producing axions today. Second, unlike solar ^{57}Fe axions, galactic ^{23}Na axions traverse the magnetic fields of the progenitor star and the galaxy, allowing some of the axions to convert to detectable gamma rays.

It is very rare for stars to synthesize odd-A isotopes in large quantities – the nuclear astrophysics favors tightly bound α -stable nuclei like C, O, and Ne – and still rarer for such isotopes, once produced, to evade rapid burn-up in $T_8 \approx 10$ stellar plasmas. ^{23}Na is an exception. The isotope is produced during carbon burning,



in the late-stage evolution of massive stars. The stars that prove to be of most interest are in the mass range of $7.5 - 15 M_\odot$, the progenitors of ONeMg white dwarfs (WDs) and of electron capture (EC) and core-collapse (CC) supernovae (SNe) [47].

The stellar input for the subsequent galactic modeling of ^{23}Na axion production was generated using the MESA code [48–53]. SN progenitors of mass 9, 10, ..., 30 were evolved through their various burning stages, including C, Ne, and O burning. The output includes the photon, neutrino (including Urca production from $^{23}\text{F}/^{23}\text{Ne}/^{23}\text{Na}$ and $^{25}\text{Ne}/^{25}\text{Na}/^{25}\text{Mg}$), and axion luminosities, as well as the radial profiles of composition and temperature at each time slice. The axion emission is computed as a function of time and radial coordinate from the ^{23}Na mass fraction and Boltzmann occupation of the $5/2^+$ 440 keV level of ^{23}Na . The axion emission rate is computed from Eq. (4), with $\omega_\gamma = 6.10 \times 10^{11}$ /sec and $\delta = 0.065$ taken from ENSDF [54].

The amount of ^{23}Na synthesized in the inner cores of these stars is large, ranging from $0.044 M_\odot$ in a $9 M_\odot$ star to $0.13 M_\odot$ in a $30 M_\odot$ one. The distributions of ^{23}Na before and after C burning are shown in Fig. 1. The core temperatures at the time ^{23}Na reaches its peak abundances range from $T_8 \approx 12$ in a $9 M_\odot$ progenitor to $T_8 \approx 24$ in a $30 M_\odot$ star. Most importantly, C burning times are much longer in lighter progenitors: in a $9 M_\odot$ SN star, burning begins when the core temperature reaches $T_8 \approx 7$ and continues for $\approx 12,500$ y. By contrast, C burning lasts about 25 y in a $30 M_\odot$ progenitor. Lower mass stars dominate 440 keV axion production because of their long C-burning times and greater abundance. The galactic 440 keV axion flux is continuous, as source durations are long compared to SN and ONeMg

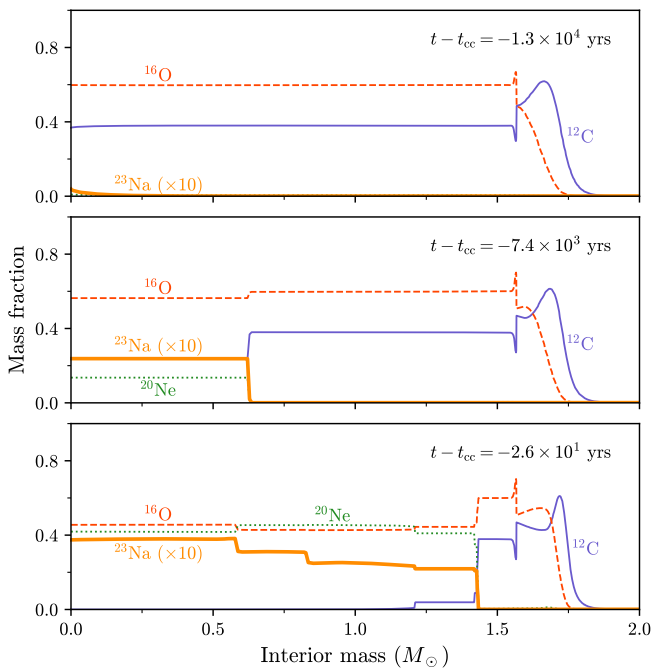


FIG. 1. Mass fractions of C, O, Ne, and ^{23}Na ($\times 10$) at the start of C+C burning (top), at the end of C burning in the innermost zone, and at the end of C burning (bottom) for a $9M_{\odot}$ SN progenitor.

WD birth rates. The Boltzmann factors are favorable: at the end of ^{23}Na synthesis in a $9M_{\odot}$ star, the 440 keV state occupation probability is 0.11.

To estimate the flux at Earth we constructed a galactic model with which we can perform Monte Carlo sampling on the position, mass, and age of contributing SN progenitors. To describe the progenitor position in the Milky Way, we use a version of the Stecker and Jones distribution [55], as parameterized in [56], to match the current inventory of SN remnants. These remnants provide a partial record of Milky Way SN activity over the last $\sim 100,000$ years. We altered this distribution to produce a nonzero remnant density in the bulge, bringing the distribution into better agreement with that of [57] near the galactic center. The distribution depends only on r (in kpc), the distance from the galactic center,

$$\rho(r) = N \left(\frac{r + 0.638}{r_{\odot}} \right)^{0.74} \exp \left(-3.54 \frac{(r - r_{\odot})}{r_{\odot}} \right) \quad (7)$$

where $r_{\odot} \approx 8.5$ kpc. The constant N is fixed by the requirement that $\rho(r)$ be a probability density.

Because we treat a flux that falls off as $1/r^2$, the thickness of the disk must be included to keep integrations well behaved. We describe the z -dependence by

$$P(z) = \frac{1}{2h} \exp \left(-\frac{|z|}{h} \right) \quad (8)$$

setting the scale height $h = 0.4$ kpc while placing the Earth at the midpoint of the disk. While our approach is

reasonable given other uncertainties, improvements could be made by adapting more sophisticated galactic models that account for the nonuniform distribution of stars [58].

Progenitors with masses $\gtrsim 9.2M_{\odot}$ produce standard core-collapse (CC) SNe [47]. After completion of C burning, stars just below this cutoff develop an inert ONeMg electron-degenerate core, with several possible outcomes. Those stars that retain most of their envelopes experience electron capture (EC) on Ne, and can explode either as a thermonuclear ECSN or a CCSN [47]. We group these stars together as the SN population, using $8.5M_{\odot}$ as the lower bound on the progenitor mass (see below).

In the sampling over progenitor mass, we use an initial mass function (IMF) of the Salpeter form [59], $P(M) \propto M^{-2.35}$. To each progenitor of mass M we assign a probability given by the integral of the IMF over $M \pm 0.5M_{\odot}$. The Salpeter IMF provides a good fit to the contemporary inventory of SN remnants [60].

The sampling over time requires us to adopt a rate for SNe. Various estimates of the CCSN rate for the galaxy as a whole have been made in recent years, with typical results being $1.63 \pm 0.46/\text{century}$ (aggregated data) [61], $1.95 \pm 0.41/\text{century}$ (extragalactic survey of similar galaxies) [62], and $1.9 \pm 1.1/\text{century}$ (^{26}Al) [63]. Use of these rates is complicated by the fact that, due to the $1/r^2$ falloff of the axion flux, 50% axions detected on Earth will originate from within 2.1 kpc. The rate may be higher in the spiral arms, where our solar system resides [64]. We adopt a rate of CC and EC SNe of 2.5/century: the results below can be scaled to any other value. The time over which we integrate is set by the duration of C burning in the $9M_{\odot}$ progenitor, 12,500y. We create an ensemble of ≈ 300 progenitors that are within 12,500y of exploding, with Poisson statistics determining the actual number and distribution in time. The mass and location of each progenitor is determined by Monte Carlo. The axion flux at Earth for the ensemble is then computed. By repeating the calculation for 1000 ensembles, we determine the flux probability distribution.

A second important axion source is ONeMg white dwarfs (WDs), with masses in the range $\approx 1.1\text{--}1.4 M_{\odot}$. In the fine-grid study of [47], progenitors with masses of $7.5\text{--}9.20 M_{\odot}$ were found to produce degenerate ONeMg cores, with those with $M \geq 8.5M_{\odot}$ ending their evolution as ECSNe and those with $M \approx 7.5\text{--}8.5M_{\odot}$ becoming ONeMg WDs. Certain heavier progenitors can also evolve to ONeMg WDs depending on the description of mass loss. Because they evolve to similar final states, we represent all WD progenitors by a single star, a $11M_{\odot}$ MESA progenitor that produces a $1.134M_{\odot}$ ONeMg WD containing $\approx 0.07M_{\odot}$ of ^{23}Na . An improved approach would be to generate a finely spaced grid of progenitors, a task beyond our scope, but might be within that of the modeling program described in [47].

An ONeMg WD continues axion production for $\approx 10^4\text{y}$ after C burning [65], as gravitational energy released

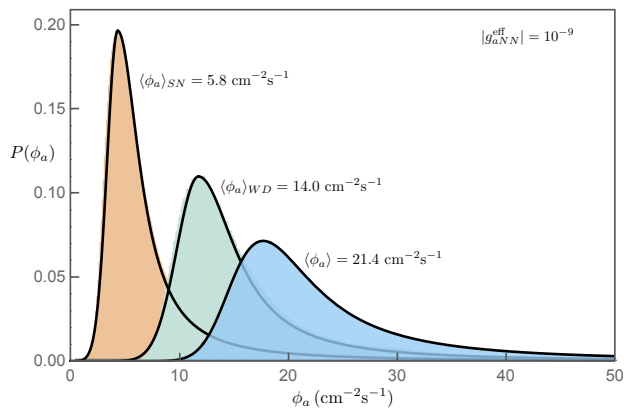


FIG. 2. From left to right, the Monte Carlo axion flux probability distributions for SN and WD sources separately, and combined. The solid lines are the analytic fits (see text).

through contraction keeps core temperatures high despite neutrino losses. This further extends the axion production, which can be five times that of comparable light SN progenitors. In our MESA calculation, axion production extends over 40,000y (15,000y) in the C burning (cooling) phase, accounting for 84% (15%) of the axion fluence.

Given a ONeMg WD birth rate, one can calculate the galactic production, just as was done for SNe. For the ONeMg WD progenitor mass range of [47], $7.5\text{--}8.5M_{\odot}$, the IMF and SN rate can be combined to yield a birth rate of $1/175\text{y}$. Alternatively, the star formation rate of $\approx 1/1.9\text{y}$ and estimated heavy ($1.1\text{--}1.4M_{\odot}$) WD fraction (1–2%) [66] together yield a birth rate of $1/(100\text{--}200)\text{y}$. In our simulations we use $1/175\text{y}$ as a representative rate.

The resulting SN and WD flux probabilities $P(\phi_a)$ computed for $g_{aNN}^{\text{eff}} = 10^{-9}$ are shown in Fig. 2. As several hundred progenitors contribute, the distributions have defined lower boundaries. However, the high-flux tails are extended, reflecting the random nature of near-Earth sources. The Monte Carlo results can be approximated by a two-sided Gaussian-Lorentzian

$$P(\phi_a) = \sqrt{\frac{\pi}{2}} \frac{1}{\sigma_1 + \sigma_2} \begin{cases} e^{-(\phi_a - \phi_0)^2/2\sigma_1^2} & \phi_a < \phi_0 \\ \left[1 + \pi \frac{(\phi_a - \phi_0)^2}{2\sigma_2^2}\right]^{-1} & \phi_a > \phi_0 \end{cases} \quad (9)$$

where ϕ_0 is the most probable flux. We find $\{\phi_0, \sigma_1, \sigma_2\} = \{11.8, 1.99, 5.32\}$, $\{4.28, 0.98, 3.08\}$, and $\{17.3, 2.63, 8.52\} \text{ cm}^{-2}\text{s}^{-1}$ for the SN, WD, and total fluxes, respectively. Because the probability profile is skewed, we will use the median to define a representative flux for the exploratory study below, $\langle \phi_a \rangle = 21.4 \text{ cm}^{-2}\text{s}^{-1}$.

Despite the lower birthrate of ONeMg WDs, they account for $\approx 70\%$ of the flux because of their long duration. σ_1 and σ_2 determine the probabilities of measuring a flux above or below the most probable value ϕ_0 , respectively. As $\sigma_2 \gg \sigma_1$, a measurement is more

likely to find a value in the Lorentzian tail than otherwise.

ALP conversion in the galactic magnetic field: Naively one expects a galactic flux of axions to be less important than a solar flux by $(d_{\text{sun}}/d_{\text{gal}})^2 \approx 10^{-19}$. In fact, the factors previously discussed yield a galactic ^{23}Na to solar ^{57}Fe flux ratio at Earth of $1/350$ (KSVZ couplings). When in addition one considers the conversion of light ALPS to detectable γ s, the factor $(B_T d)^2$ swings the balance sharply in favor of the galaxy, which enjoys an advantage of $\approx 10^{17}$ over the 9.26 m, 9 T CAST magnet.

^{23}Na axions arrive on Earth after transiting both the local magnetic field of the progenitor and that of the galaxy. Magnetic fields can convert the axions to 440 keV γ s through the coupling

$$\mathcal{L} = -g_{a\gamma\gamma} \vec{E} \cdot \vec{B}_a \quad (10)$$

The CAST limit on $g_{a\gamma\gamma}$ is [67]

$$|g_{a\gamma\gamma}| < 0.66 \times 10^{-10} \text{ (95\% C.L.) for } m_a \lesssim 0.02 \text{ eV.} \quad (11)$$

Constraints from axion energy loss in horizontal branch and AGB star produce similar bounds [24, 25]. Tighter limits have been established by ADMX [7–9] and from analyses of the TeV γ -ray source Markarian 421 [68], but they are valid only in specific mass ranges.

As axion couplings to quarks and gluons also imply axion-pion mixing, one expects $|g_{a\gamma\gamma}| \sim (\alpha/m_N)|g_{aNN}|$. For the KSVZ axion, this relates a coupling of the size used here $|g_{app}| \sim 10^{-9}$ to $|g_{a\gamma\gamma}| \sim 4.9 \times 10^{-12} \text{ GeV}^{-1}$. Consequently, in the work below, we take the nominal value of $g_{a\gamma\gamma}$ to be 5×10^{-12} , placing both couplings near their current experimental limits. Observational signals are governed by $|g_{aNN}^{\text{eff}} g_{a\gamma\gamma}|$, which then has the nominal value 5×10^{-21} . We will explore below the potential of COSI to probe couplings below this nominal value.

The conversion probability of very light ^{23}Na ALPs to γ s depends on the component of the galactic magnetic field perpendicular to the ALP’s direction. Both the in-plane transverse component and that perpendicular to the Milky Way disk contribute. Here we simplify, taking the total transverse component to be constant at $B_T \approx 1 \mu\text{G}$. This choice is consistent with retaining just the disk-perpendicular component of the “logistic” parameterization from Fig. 16 of [69].

For an axion of energy E traveling a distance d through a homogeneous field, the conversion probability is [70]

$$P_{a \rightarrow \gamma} = (\Delta_{a\gamma} d)^2 \frac{\sin^2(\Delta_{\text{osc}} d/2)}{(\Delta_{\text{osc}} d/2)^2} \quad (12)$$

where $\Delta_{\text{osc}} = [(\Delta_a - \Delta_{\text{pl}})^2 + 4\Delta_{a\gamma}^2]^{1/2}$, $\Delta_{a\gamma} = g_{a\gamma\gamma} B_T/2$, $\Delta_a = -m_a^2/2E$, and $\Delta_{\text{pl}} = -\omega_{\text{pl}}^2/2E$. Using an galactic electron density $n_e \approx 1.1 \times 10^{-2} \text{ cm}^{-3}$, we obtain the plasma frequency $\omega_{\text{pl}} = \sqrt{4\pi\alpha n_e/m_e} \approx$

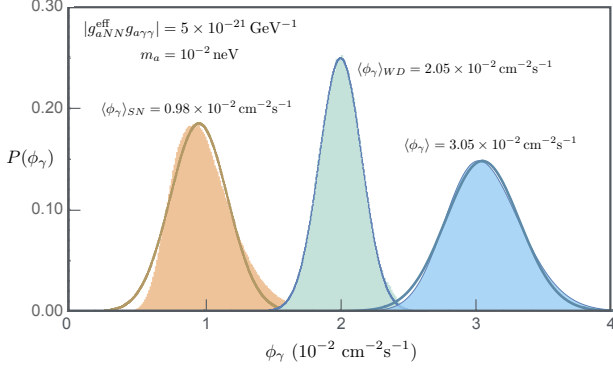


FIG. 3. As in Fig 2, but for the conversion γ s. The Monte Carlo results are shown with simple Gaussian fits (solid lines).

3.9×10^{-12} eV. The various terms can be expressed parametrically as

$$\begin{aligned} \Delta_a &= -7.8 \times 10^{-3} \times \left(\frac{m_a}{10^{-11} \text{ eV}} \right)^2 \left(\frac{E}{\text{MeV}} \right)^{-1} \text{ kpc}^{-1} \\ \Delta_{\text{pl}} &= -1.1 \times 10^{-3} \times \left(\frac{E}{\text{MeV}} \right)^{-1} \text{ kpc}^{-1} \\ \Delta_{a\gamma} &= 1.5 \times 10^{-2} \times \left(\frac{g_{a\gamma\gamma}}{10^{-11} \text{ GeV}^{-1}} \right) \left(\frac{B_T}{10^{-6} \text{ G}} \right) \text{ kpc}^{-1} \end{aligned} \quad (13)$$

The γ -ray flux is obtained by repeating the Monte Carlo galaxy simulation with the conversion probability included. Unlike the axion flux, where nearby sources are especially important, the additional factor of d^2 from Eq. (12) leads to a source weighting proportional to the number of sources at a distance d , favoring distant sources. The contribution within a given solid angle is then proportional to the number of stars in the associated cone.

The γ -ray flux probability distributions are shown in Fig. 3 for a light ALP ($m_a = 10^{-11}$ eV). We find $\langle \phi_\gamma \rangle \approx 3.05 \times 10^{-2} \text{ cm}^{-2} \text{ s}^{-1}$ and a conversion probability $\langle P_{a \rightarrow \gamma} \rangle \approx 0.0013$. $P(\phi_\gamma)$ is well described by a Gaussian (see Fig. 3) with $\sigma \approx 0.27 \times 10^{-2} \text{ cm}^{-2} \text{ s}^{-1}$. As the conversion occurs far from the axion source, the γ line profile should be narrow, with a Gaussian width of ≈ 0.9 keV, reflecting the thermal line broadening of their axion parents.

γ -ray detection with the COSI detector: COSI's planned launch is 2027 [41]. As an all-sky detector, it is optimized for continuous γ -ray sources at ≈ 1 MeV. From Fig. 2(a) of [41] we obtain a COSI narrow-line point source sensitivity of $6 \times 10^{-6} \text{ cm}^{-2} \text{ s}^{-1}$ (3σ) at 440 keV after two years of survey time. This sensitivity can be adapted to the case of multiple point sources by accounting for the background noise scaling of $\sqrt{\Omega/\Omega_0}$, where Ω_0 is the solid angle subtended by a 4° cone, COSI's resolution. This cone spans the effective height of the galactic plane, but not the distribution within the plane: as 90% of the signal

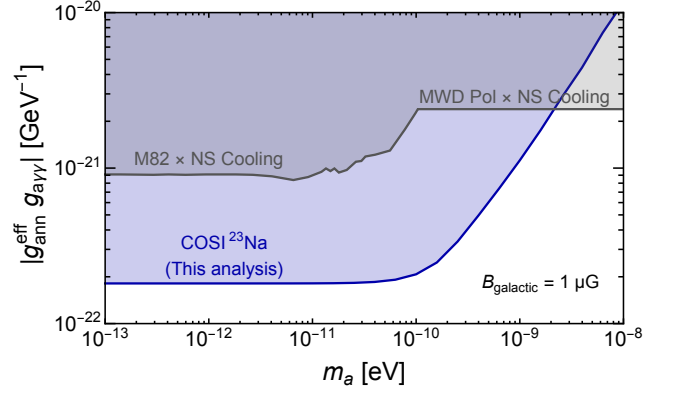


FIG. 4. Expected 3σ limit on the ALP coupling $|g_{aNN}^{\text{eff}} g_{a\gamma\gamma}|$ from a COSI search for ^{23}Na $a \rightarrow \gamma$ conversion, after two years of surveying (blue shaded). The other constraints shown (gray shaded) were obtained by combining leading limits on $g_{a\gamma\gamma}$, from axion-photon conversion in M82 and axion-induced polarization measurements in magnetic white dwarfs [71, 72], with the bound on g_{aNN}^{eff} obtained from isolated neutron star cooling [73].

comes from the hemisphere toward the galactic center, we estimate that $\sqrt{\Omega/\Omega_0} \approx 6.7$, yielding an effective COSI sensitivity to ^{23}Na conversion γ s of $4 \times 10^{-5} \text{ cm}^{-2} \text{ s}^{-1}$ (3σ). Our naive analysis makes no use of the potentially helpful correlation of signal with angular stellar density.

Figure 4 shows the resulting bounds on the ALP coupling $|g_{aNN}^{\text{eff}} g_{a\gamma\gamma}|$ as a function of the ALP mass. A COSI sensitivity of $4 \times 10^{-5} \text{ cm}^{-2} \text{ s}^{-1}$ will probe $|g_{aNN}^{\text{eff}} g_{a\gamma\gamma}|$ to $1.8 \times 10^{-22} \text{ GeV}^{-1}$ for sufficiently light ALP masses ($m_a \lesssim 0.1$ eV). This limit corresponds to a 3σ detection at the level defined by $\langle \phi_\gamma \rangle$. The figure also shows the $|g_{aNN}^{\text{eff}} g_{a\gamma\gamma}|$ constraints that can be obtained by combining the leading astrophysical bounds on $g_{a\gamma\gamma}$, from axion-photon conversion in M82 and axion-induced polarization measurements in magnetic white dwarfs [71, 72], with the bound on $g_{aNN}^{\text{eff}} = g_{\text{app}} - 0.062 g_{\text{ann}}$ obtained from the cooling of isolated neutron stars [73].

Outlook: The conversion γ s from galactic ^{23}Na axions appear to be an interesting target for COSI and similar all-sky detectors. There are further issues to be explored. First, the exploratory calculations that we have performed could be improved by utilizing more sophisticated models of the star [58] and magnetic field [69] distributions. Second, axion interactions with the progenitor's magnetic field can enhance the $a \rightarrow \gamma$ conversion, extending sensitivities to heavier ALPs [74]. As much is known about the distribution of field strengths in WDs, this physics could be incorporated into the Monte Carlo study. Third, axion emission during C burning can affect progenitor evolution. While our preliminary studies suggest that the effects are important only if $|g_{aNN}^{\text{eff}}| \gtrsim 10^{-8}$, still this should be

quantified.

We thank Steve Boggs, Liang Dai, Chris Fryer, Georg Raffelt, Josiah Schwab, and Stan Woosley for helpful discussions. We thank the MESA Collaboration for their open source software; our modifications are documented on GitHub [75]. WH and AR are supported through the NSF cooperative agreement 2020275. WH is also supported by the US DOE (DE-SC0004658 and DE-SC0023663) and by the Heising-Simons Foundation (00F1C7). The progenitor modeling was performed by AM (2023) and XL (2024) as undergraduate research projects for the NSF Center N3AS.

^a haxton@berkeley.edu

^b xingyzt@berkeley.edu

^c amccutcheon@ucdavis.edu

^d anupam.ray@berkeley.edu

- [1] R. D. Peccei and H. R. Quinn, *Phys. Rev. Lett.* **38**, 1440 (1977).
- [2] S. Weinberg, *Phys. Rev. Lett.* **40**, 223 (1978).
- [3] F. Wilczek, *Phys. Rev. Lett.* **40**, 279 (1978).
- [4] P. Sikivie, *Phys. Rev. Lett.* **51**, 1415 (1983).
- [5] P. Sikivie, *Rev. Mod. Phys.* **93**, 015004 (2021).
- [6] S. Asztalos *et al.*, *Phys. Rev. D* **64**, 092003 (2001).
- [7] N. Du *et al.* (ADMX Collaboration), *Phys. Rev. Lett.* **120**, 151301 (2018).
- [8] T. Braine *et al.* (ADMX Collaboration), *Phys. Rev. Lett.* **124**, 101303 (2020).
- [9] C. Bartram *et al.* (ADMX Collaboration), *Phys. Rev. Lett.* **127**, 261803 (2021).
- [10] L. Zhong *et al.*, *Phys. Rev. D* **97**, 092001 (2018).
- [11] L. Brouwer *et al.* (DMRadio Collaboration), *Phys. Rev. D* **106**, 103008 (2022).
- [12] C. P. Salemi *et al.*, *Phys. Rev. Lett.* **127**, 081801 (2021).
- [13] D. Budker, P. W. Graham, M. Ledbetter, S. Rajendran, and A. O. Sushkov, *Phys. Rev. X* **4**, 021030 (2014).
- [14] A. P. Quiskamp *et al.*, “Near-quantum limited axion dark matter search with the organ experiment around $26 \mu\text{eV}$,” (2024), arXiv:2407.18586 [hep-ex].
- [15] D. Page, M. Prakash, J. M. Lattimer, and A. W. Steiner, *Phys. Rev. Lett.* **106**, 081101 (2011).
- [16] P. S. Shternin, D. G. Yakovlev, C. O. Heinke, W. C. G. Ho, and D. J. Patnaude, *Monthly Notices of the Royal Astronomical Society: Letters* **412**, L108 (2011).
- [17] L. B. Leinson, *Physics Letters B* **741**, 87 (2015).
- [18] L. B. Leinson, *Journal of Cosmology and Astroparticle Physics* **2014**, 031 (2014).
- [19] K. Hamaguchi, N. Nagata, K. Yanagi, and J. Zheng, *Phys. Rev. D* **98**, 103015 (2018).
- [20] L. B. Leinson, *JCAP* **09**, 001 (2021).
- [21] M. Buschmann, C. Dessert, J. W. Foster, A. J. Long, and B. R. Safdi, *Phys. Rev. Lett.* **128**, 091102 (2022).
- [22] A. Sedrakian, *Phys. Rev. D* **93**, 065044 (2016).
- [23] A. Sedrakian, *Phys. Rev. D* **99**, 043011 (2019).
- [24] A. Caputo and G. Raffelt, *PoS COSMICWISPerS*, 041 (2024), arXiv:2401.13728 [hep-ph].
- [25] P. Carezza, M. Giannotti, J. Isern, A. Mirizzi, and O. Straniero, *Phys. Rept.* **1117**, 1 (2025), arXiv:2411.02492 [hep-ph].
- [26] G. G. Raffelt, *Lect. Notes Phys.* **741**, 51 (2008), arXiv:hep-ph/0611350.
- [27] T. Fischer, S. Chakraborty, M. Giannotti, A. Mirizzi, A. Payez, and A. Ringwald, *Phys. Rev. D* **94**, 085012 (2016).
- [28] J. H. Chang, R. Essig, and S. D. McDermott, *J. High Energy Phys.* **2018**, 51 (2018).
- [29] P. Carezza, T. Fischer, M. Giannotti, G. Guo, G. Martinez-Pinedo, and A. Mirizzi, *JCAP* **10**, 16 (2019).
- [30] P. Carezza, B. Fore, M. Giannotti, A. Mirizzi, and S. Reddy, *Phys. Rev. Lett.* **126**, 071102 (2021).
- [31] W. C. Haxton and K. Y. Lee, *Phys. Rev. Lett.* **66**, 2557 (1991).
- [32] M. S. Turner, *Physics Reports* **197**, 67 (1990).
- [33] S. Moriyama, *Phys. Rev. Lett.* **75**, 3222 (1995).
- [34] S. Andriamonje *et al.* (CAST Collaboration), *Journal of Cosmology and Astroparticle Physics* **2009**, 002 (2009).
- [35] M. Krcmar, Z. Krecak, M. Stipcevic, A. Ljubicic, and D. A. Bradley, *Phys. Letts. B* **442**, 38 (1998).
- [36] T. Namba, *Physics Letters B* **645**, 398 (2007).
- [37] A. V. Derbin, V. N. Muratova, D. A. Semenov, and E. V. Unzhakov, *Physics of Atomic Nuclei* **74**, 596 (2011).
- [38] F. Alessandria *et al.* (CUORE), *JCAP* **05**, 007 (2013), arXiv:1209.2800 [hep-ex].
- [39] L. Di Luzio *et al.*, *Eur. Phys. J. C* **82**, 120 (2022), arXiv:2111.06407 [hep-ph].
- [40] L. Fleury, I. Caiazzo, and J. Heyl, *Phys. Rev. D* **107**, L101303 (2023), arXiv:2208.00405 [astro-ph.HE].
- [41] J. A. Tomsick *et al.*, *PoS ICRC2023*, 745 (2023), arXiv:2308.12362 [astro-ph.HE].
- [42] J. E. Kim, *Phys. Rev. Lett.* **43**, 103 (1979).
- [43] M. Shifman, A. Vainshtein, and V. Zakharov, *Nuclear Physics B* **166**, 493 (1980).
- [44] M. Dine, W. Fischler, and M. Srednicki, *Physics Letters B* **104**, 199 (1981).
- [45] A. P. Zhitnitskii, *Sov. J. Nucl. Phys. (Engl. Transl.; (United States)* **31:2** (1980).
- [46] G. G. di Cortona, E. Hardy, and J. P. Vega, *J. High Energy Physics* **2016**, 34 (2016).
- [47] M. Limongi, L. Roberti, A. Chieffi, and K. Nomoto, *The Astrophysical Journal Supplement Series* **270**, 29 (2024).
- [48] B. Paxton, L. Bildsten, A. Dotter, F. Herwig, P. Lesaffre, and F. Timmes, *Astrophys. J. Suppl.* **192**, 3 (2011), arXiv:1009.1622 [astro-ph.SR].
- [49] B. Paxton *et al.*, *Astrophys. J. Suppl.* **208**, 4 (2013), arXiv:1301.0319 [astro-ph.SR].
- [50] B. Paxton *et al.*, *Astrophys. J. Suppl.* **220**, 15 (2015), arXiv:1506.03146 [astro-ph.SR].
- [51] B. Paxton *et al.*, *Astrophys. J. Suppl.* **234**, 34 (2018), arXiv:1710.08424 [astro-ph.SR].
- [52] B. Paxton *et al.*, *Astrophys. J. Suppl.* **243**, 10 (2019), arXiv:1903.01426 [astro-ph.SR].
- [53] A. S. Jermyn *et al.*, *Astrophys. J. Suppl.* **265**, 15 (2023), arXiv:2208.03651 [astro-ph.SR].
- [54] M. Shamsuzzoha Basunia and A. Chakraborty, *Nuclear Data Sheets* **171**, 1 (2021).
- [55] F. W. Stecker and F. C. Jones, *Astrophys. J.* **217**, 843 (1977).
- [56] S. Verberne and J. Vink, *Mon. Not. Roy. Astron. Soc.* **504**, 1536 (2021), arXiv:2103.16973 [astro-ph.GA].
- [57] G. L. Case and D. Bhattacharya, *Astrophys. J.* **504**, 761 (1998).
- [58] M. Kachelriess and V. Mikalsen, *Comp. Phys. Comm.*

- 311**, 109537 (2025).
- [59] E. E. Salpeter, *Astrophys. J.* **121**, 161 (1955).
- [60] B. F. Williams, T. J. Hillis, J. W. Murphy, K. Gilbert, J. J. Dalcanton, and A. E. Dolphin, *Astrophys. J.* **860**, 39 (2018).
- [61] K. Rozwadowska, F. Vissani, and E. Cappellaro, *New Astronomy* **83**, 101498 (2021).
- [62] N. Aghanim *et al.* (Planck Collaboration), *A&A* **641**, A6 (2020).
- [63] R. Diehl *et al.*, *Nature* **439**, 45 (2006).
- [64] P. M. Dragicevich, D. G. Blair, and R. R. Burman, *Monthly Notices of the Royal Astronomical Society* **302**, 693 (1999).
- [65] M. E. Camisassa *et al.*, *A&A* **625**, A87 (2019).
- [66] T. Cunningham, P.-E. Tremblay, and M. W. O'Brien, *MNRAS* **527**, 3602 (2023).
- [67] V. Anastassopoulos *et al.* (CAST Collaboration), *Nature Physics* **13**, 584 (2017).
- [68] H.-J. Li, W. Chao, and Y.-F. Zhou, *Physics Letters B* **858**, 139075 (2024).
- [69] M. Unger and G. R. Farrar, *The Astrophysical Journal* **970**, 95 (2024).
- [70] G. Raffelt and L. Stodolsky, *Phys. Rev. D* **37**, 1237 (1988).
- [71] O. Ning and B. R. Safdi, *Phys. Rev. Lett.* **134**, 171003 (2025), [arXiv:2404.14476 \[hep-ph\]](https://arxiv.org/abs/2404.14476).
- [72] J. N. Benabou, C. Dessert, K. C. Patra, T. G. Brink, W. Zheng, A. V. Filippenko, and B. R. Safdi, (2025), [arXiv:2504.12377 \[hep-ph\]](https://arxiv.org/abs/2504.12377).
- [73] M. Buschmann, C. Dessert, J. W. Foster, A. J. Long, and B. R. Safdi, *Phys. Rev. Lett.* **128**, 091102 (2022), [arXiv:2111.09892 \[hep-ph\]](https://arxiv.org/abs/2111.09892).
- [74] C. A. Manzari, Y. Park, B. R. Safdi, and I. Savoray, *Phys. Rev. Lett.* **133**, 211002 (2024).
- [75] X. Liu, "Stellar axion simulation," (2025), <https://github.com/xingyzt/saltyaxions>.